



## RESEARCH ARTICLE

10.1029/2021JD035199

# Stratospheric Adiabatic Mixing Rates Derived From the Vertical Gradient of Age of Air

Marianna Linz<sup>1</sup> , R. Alan Plumb<sup>2</sup> , Aman Gupta<sup>3</sup> , and Edwin P. Gerber<sup>4</sup> 

<sup>1</sup>Department of Earth and Planetary Sciences and School of Engineering and Applied Sciences, Harvard University, Cambridge, MA, USA, <sup>2</sup>Department of Earth, Atmospheric and Planetary Sciences, Emeritus, Massachusetts Institute of Technology, Cambridge, MA, USA, <sup>3</sup>Meteorological Institute Munich, Ludwig Maximilian University, Munich, Germany, <sup>4</sup>Courant Institute of Mathematical Sciences, New York University, New York, NY, USA

### Key Points:

- A new metric for adiabatic mixing in the stratosphere is developed from the age of air tracer
- We examine hemispheric asymmetry and discuss the slow time evolution of the flow
- We calculate this metric to perform a preliminary comparison between models and satellite data

### Correspondence to:

M. Linz,  
[mllinz@seas.harvard.edu](mailto:mllinz@seas.harvard.edu)

### Citation:

Linz, M., Plumb, R. A., Gupta, A., & Gerber, E. P. (2021). Stratospheric adiabatic mixing rates derived from the vertical gradient of age of air. *Journal of Geophysical Research: Atmospheres*, 126, e2021JD035199. <https://doi.org/10.1029/2021JD035199>

Received 4 MAY 2021  
Accepted 22 SEP 2021

**Abstract** The circulation of the stratosphere transports important trace gases, including ozone, and can be thought of as having a fast horizontal mixing component and a slow meridional overturning component. Measuring the strength of the circulation directly is not possible, and so it must be inferred from tracer measurements. Long-lived trace gases can be related to the idealized tracer age of air, which describes how long an air parcel has been in the stratosphere. In this paper, we derive a quantitative relationship between the vertical gradient of age and the horizontal mixing between the tropics and the extratropics using a “leaky pipe” framework in isentropic coordinates. Mixing rates of air into and out of the tropics are related to the vertical gradient of age in the tropics and in the extratropics, respectively. The derivation is repeated with the hemispheres separated so that the vertical structure of the mixing in the two hemispheres can be compared directly. These theories are applied to output from an idealized model of the stratosphere and from a realistic chemistry-climate model to test our assumptions and calculate the mixing rates in the models. We then perform a quantitative comparison of the mixing rates in the Northern and Southern hemispheres along with an examination of where such a separation is valid. Finally, we perform a very preliminary calculation of mixing efficiency with satellite data to demonstrate the use of the mixing metric to compare mixing in models and data.

## 1. Introduction

Understanding the circulation of the stratosphere has developed through observations of trace gases, and in particular ozone (Dobson et al., 1929) and water vapor (Brewer, 1949). Both Dobson and Brewer surmised that upward motion in the tropics, followed by slow, poleward movement and downwelling in the extratropics would be consistent with the observed trace gas distributions. Neither meridional motion on a rotating sphere nor vertical motion through a stratified fluid is easily achieved, however; meridional motion requires a torque and vertical motion requires diabatic heating. Both of these are provided by the deposition of pseudomomentum by the breaking of planetary-scale waves in the stratosphere. These breaking waves also cause a substantial amount of stirring within the isentropic layers; indeed, this is the dominant effect. This behavior provides the most basic picture of stratospheric circulation: Wave breaking drives rapid isentropic motions, and it also causes slow vertical and poleward motion (Plumb, 2002). The mean mass transport within the stratosphere has come to be known as the Brewer–Dobson Circulation (BDC) (Butchart, 2014).

Over 70 years after Brewer’s paper, many inferences about the strength and variability of the stratospheric circulation are still tracer-based. Although estimates of trends in the BDC have been calculated from satellite temperature observations (Fu et al., 2015), even this calculation relied on ozone and water vapor data. Tracking the vertical propagation of the seasonal variations in water vapor concentrations is one example of using tracer observations to understand the BDC and mixing (e.g., Glanville & Birner, 2017). Variations in lower stratospheric water vapor concentrations are also linked to large-scale changes in the circulation on interannual timescales (Randel et al., 2006). Recent work has also suggested using a combination of many trace gases and inverting a large suite of observations to find a best fit solution (von Clarmann & Grabowski, 2016), although this has yet to be effectively applied in practice.

Although chemical tracers can be observed directly, a theoretical tracer is also useful for thinking about the stratospheric circulation. The idealized tracer “age of air” is a measure of how long a parcel of air has been in the stratosphere (Hall & Plumb, 1994) and contains the average history of the trajectories of the bits of

© 2021 The Authors.

This is an open access article under the terms of the [Creative Commons Attribution-NonCommercial License](https://creativecommons.org/licenses/by-nc/4.0/), which permits use, distribution and reproduction in any medium, provided the original work is properly cited and is not used for commercial purposes.

air that make up the parcel. Age of air has a zero boundary condition at the tropopause and a unit source as long as it is in the stratosphere, or it can be formulated in terms of a tracer that is conserved in the stratosphere and has a source in the troposphere that is linearly increasing in time (Boering et al., 1996). Although this is just replacing one idealized tracer with another, the linearly increasing tracer is far more realistic.

It is necessary to approximate age from observations because no species has a constant growth rate or is perfectly conserved; sulfur hexafluoride ( $\text{SF}_6$ ) and carbon dioxide ( $\text{CO}_2$ ) are approximately linearly increasing, but  $\text{SF}_6$  has a mesospheric sink and  $\text{CO}_2$  has a strong seasonal cycle. To convert these real tracers to the idealized age tracer, certain assumptions must be made about the overall distribution of ages that are represented in the observed sample (Waugh & Hall, 2002). The details of how age of air is calculated from tracers can change whether the in situ measurements from the past 40 years show a trend or not (Fritsch et al., 2020). A suite of chemical tracers could be used to constrain the age distribution with certain constraints for its form (Andrews, Boering, et al., 2001; Andrews et al., 1999; Ehhalt et al., 2007; Hauck et al., 2019; Schoeberl et al., 2005). However, distinct tracers do not necessarily provide distinct degrees of freedom, since long-lived tracers all have compact relationships with each other (Plumb, 2007). Moreover, real physical links between the circulation and the tracers are somewhat obfuscated by this purely data-driven approach. To best understand the stratosphere, the underlying understanding of the characteristics and physics of the BDC should be included while attempting to quantify the strength of that circulation.

The BDC consists of two branches, a deep branch associated with the dissipation of planetary scale waves in the middle and upper stratosphere, and a shallow branch associated with the breaking of synoptic and planetary waves just above the subtropical jet (Birner & Bönisch, 2011; McLandress & Shepherd, 2009; Plumb, 2002). The net zonal mean meridional mass transport is frequently expressed in the form of the Transformed Eulerian Mean (TEM) residual circulation (Andrews & McIntyre, 1976, e.g., Butchart et al., 2006; Garcia & Randel, 2008) or more rarely, the diabatic circulation (Linz et al., 2016). These treatments are mostly equivalent, depending on the choice of calculation method for the TEM residual circulation (Linz et al., 2019). The diabatic circulation has the advantage that it can be directly related to age (Linz et al., 2016), and thus calculated from global satellite tracer measurements (Linz et al., 2017).

Typical metrics for the BDC either are explicitly global or are for the tropics only, precluding separation of the two hemispheres. However, the two hemispheres should not be expected to be symmetric. The climatological wave driving in the Northern and Southern hemispheres differ (e.g., Labitzke et al., 1980; Rosenlof, 1996). Furthermore, long-term variability in the two hemispheres also differs; with the development of the ozone hole in the Southern Hemisphere until year 2000 and then the subsequent, erratic, and ongoing recovery (Solomon et al., 2016), asymmetric long-term variability seems rather likely (Polvani et al., 2019). Moreover, observations of the time evolution of certain trace gases suggest such asymmetric changes in the circulation (Mahieu et al., 2014). These factors all indicate a need for tracer-based, quantitative metrics for the circulation that can separate the variability in the two hemispheres.

The wave breaking that drives the meridional flow also causes turbulent, irreversible mixing (McIntyre & Palmer, 1984), sometimes referred to as “two-way mixing” because of the two-way mass exchange between the tropics and the midlatitudes (Garny et al., 2014). Stratospheric mixing is quite uncertain, with state of the art models disagreeing by at least a factor of two by one metric (Dietmüller et al., 2018). Previous studies of mixing have used two main approaches: (a) treating mixing as a diffusivity (Allen & Nakamura, 2001; Haynes & Shuckburgh, 2000; Leibensperger & Plumb, 2014; Newman et al., 1986) and (b) using the age of air to infer some metric of mixing (Garny et al., 2014; Moore et al., 2014; Ploeger, Abalos, et al., 2015; Ploeger, Riese, et al., 2015; Ray et al., 2010, 2014, 2016). The present work will also use age and so a brief summary of the latter is in order.

In the calculation of “Aging by Mixing” (Garny et al., 2014; Ploeger, Abalos, et al., 2015; Ploeger, Riese, et al., 2015), the age of air calculated from an ideal age tracer in a model is compared to the age that air would be if it were to simply age at a constant rate following the TEM residual circulation streamfunction, and the difference is surmised to be due to mixing. This creates a two-dimensional zonal mean structure of “Aging by Mixing,” which clearly demonstrates that age reflects both the residual circulation and mixing. Beyond qualitative comparisons, however, this two-dimensional field is difficult to interpret, and this method is useful for models only. Another age-based technique used to examine mixing adapts the Tropical

Leaky Pipe (TLP) of Neu and Plumb (1999) to look at mixing efficiency and to understand the impact of mixing on age (Moore et al., 2014; Ray et al., 2010, 2014, 2016). The TLP model envisions a well-mixed “tropical pipe” that is relatively isolated from the well-mixed extratropics with a constant vertical velocity in the tropics and a constant mixing efficiency between the two regions. Its vertical coordinate is height, which has the advantage of being physically intuitive. The adaptations of the model have relaxed some of the assumptions, allowing for vertical variations in the vertical velocity, and have incorporated multiple trace gases. The studies by Ray et al. (2014) and Ray et al. (2016) include running the TLP with Lagrangian forward particle trajectories to be able to examine the full age spectra and mixing. These various approaches to mixing yield quantitatively different results, as they are quantifying different (though related) things.

More recently, the isentropic age-budget theory proposed in Linz et al. (2016) and in this paper has been applied to quantify and compare differences in stratospheric transport among state of the art primitive equation solvers (a.k.a. dynamical cores). An intermodel stratospheric transport benchmark test (proposed in Gupta et al., 2020) revealed a strong impact of numerics on transport. Modern cores with different numerics were identically forced at varying resolutions, but were found to converge toward different stratospheric circulation and strikingly different stratospheric age. A following study (Gupta et al., 2021) aimed at understanding this spread in age, used the theory along with a numerically integrated TLP with vertically varying parameters estimated from models to isolate the contribution of each process (diabatic circulation, isentropic mixing, and numerical diffusion) toward the spread. The study found a strong tropical control on stratospheric tracer transport and concluded that persisting differences in the model representation of both diabatic circulation and mixing, even at high resolution, can lead to a significant intermodel spread in stratospheric trace gas transport.

In this paper, we seek to provide a comprehensive description of the stratospheric circulation in terms of age. We derive a new relationship between the age of air and the circulation analytically based on the TLP framework in isentropic coordinates. The use of isentropic coordinates allows for a straightforward separation of the diabatic circulation from the adiabatic mixing. This is an extension of the theory developed for the diabatic circulation in Linz et al. (2016), and this theory also requires neither model runs nor Lagrangian trajectory calculations for calculating metrics of stratospheric transport.

We derive a theory to calculate the mean adiabatic mixing at every level using the vertical gradient of age (Section 2) in separate hemispheres, thus improving upon the TLP model by considering vertical variations in mixing and in vertical velocity. In Section 4, we apply the theory to output from an idealized and a comprehensive model (described in Section 3), and we show the circumstances under which the hemispheres can be treated separately. Critically, the mixing metric can be calculated from observations, and with numerous caveats about the limitations of both the theory and especially the data, we do so using satellite data in Section 5. Implications and limitations of this study are discussed in Section 6.

## 2. Theory

Linz et al. (2016) related the age of air on an isentropic surface to the mass flux through that surface. Starting from the ideal age equation, assuming steady state and neglecting diabatic diffusion, they showed that the difference in the mass-flux-weighted age of downwelling and upwelling air on an isentropic surface is equal to the ratio of total mass above that surface to the total diabatic overturning flux through that surface:

$$\Delta\Gamma = M/\mathcal{M}. \quad (1)$$

$\Delta\Gamma = \Gamma_d - \Gamma_u$  is the difference in mass-flux-weighted age averaged over the downwelling and upwelling regions,  $M$  is the total mass above the isentrope, and  $\mathcal{M}$  is the overturning mass flux through the isentrope. This is related to the TLP of Neu and Plumb (1999), who divided the stratosphere into “tropics” and “extratropics” based on the edge of the surf zone rather than the zero in upwelling. The key to establishing a parallel relationship to the TLP is to define the ages with a mass-flux weighting. The mass-flux-weighted downwelling and upwelling ages,  $\Gamma_d$  and  $\Gamma_u$  respectively, are defined:

$$\Gamma_u(\theta) = \left[ \int_{up} \sigma \dot{\theta} dA \right]^{-1} \int_{up} \sigma \dot{\theta} \Gamma dA, \quad (2)$$

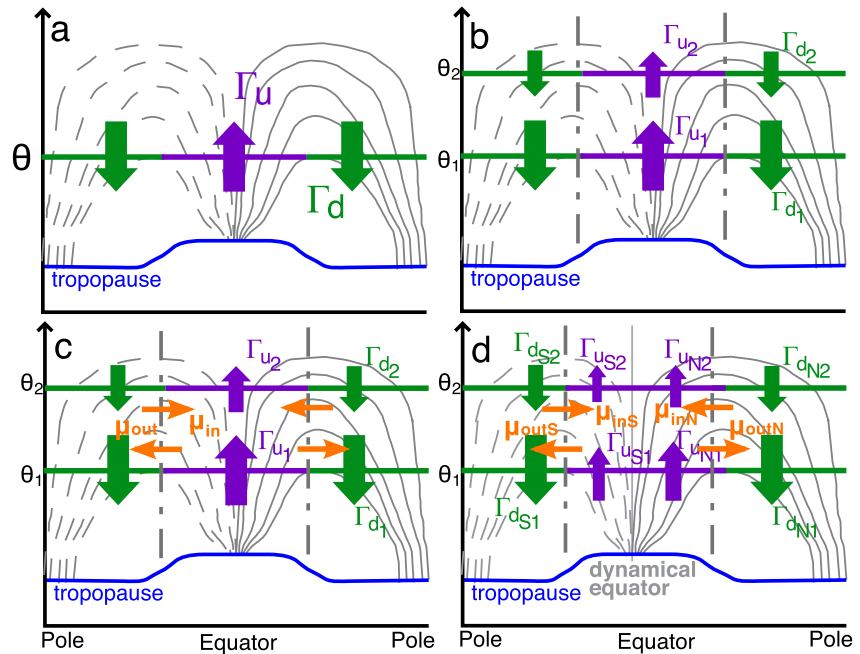


**Figure 1.** Schematics of the stratospheric circulation: (a) global circulation in dotted and thin solid lines through one isentrope, with upwelling region shown in purple and downwelling regions shown in green. Upwelling and downwelling mass fluxes are shown in purple and green arrows, respectively, and have a mass-flux-weighted mean age of  $\Gamma_u$  and  $\Gamma_d$ . (b) as before, but with an additional isentropic layer shown. The dash-dot lines represent the edges of the tropical pipe or the turnaround latitudes. This is where the diabatic vertical velocity,  $\dot{\theta}$ , is zero and they can have a varying latitude with height. (c) same as (b), but with mixing into and out of the tropics shown in orange arrows. (d) Same as in (c) but now with separate hemispheres that are divided by a dynamical equator (light gray solid line) corresponding to the zero streamline in the time mean of the circulation. Here, the Northern Hemisphere is shown as having a greater meridional extent, consistent with reanalyses. Although this diagram shows the dynamical equator as vertical, it can also vary with height.

and

$$\Gamma_d(\theta) = \left[ \int_{down} \sigma \dot{\theta} dA \right]^{-1} \int_{down} \sigma \dot{\theta} \Gamma dA. \quad (3)$$

where  $\Gamma$  is the age,  $\dot{\theta}$  is the diabatic vertical velocity,  $\sigma = -g^{-1} \partial p / \partial \theta$  is the isentropic density, and the upwelling and downwelling regions are defined as where  $\dot{\theta} > 0$  and where  $\dot{\theta} < 0$ , respectively. Integration over each region is designated by the integration limits *up* and *down*. These regions can vary in the vertical. Like Neu and Plumb (1999), we make the simplifying assumption that the air coming into the tropics has the average age of the extratropical region ( $\Gamma_d$ ), and likewise the air leaving the tropics has the average age of the tropical region ( $\Gamma_u$ ), although the definitions here are mass-flux-weighted. This assumption is one of the primary sources of error in this method. Hemispheric symmetry is implied (because both tropical boundaries are treated together).

The overturning mass flux, the diabatic circulation, is equal in the upwelling and downwelling regions in steady state and is given by

$$\int_{up} \sigma \dot{\theta} dA = - \int_{down} \sigma \dot{\theta} dA = \mathcal{M}(\theta). \quad (4)$$

These equations and definitions, repeated from Linz et al. (2016), demonstrate that the horizontal difference of age is set exclusively by the diabatic circulation. In Figure 1a, an idealized diabatic circulation streamfunction is shown in isentropic coordinates with one level that is wholly within the stratosphere highlighted. The upwelling and downwelling regions are in green and purple, respectively. Mixing has no role in setting the difference in age along the isentropic surface, but mixing will be critical in determining the vertical gradient.

In what follows, we show that that the vertical (cross-isentropic) gradient of age is related to the adiabatic mixing, with the assumption of steady state and neglecting diabatic diffusion.

### 2.1. Vertical Tropical Age Gradient

Consider the schematic in Figure 1b. A second isentropic surface is now highlighted (Both  $\theta_1$  and  $\theta_2$  are wholly within the stratosphere). The regions where the vertical velocity,  $\dot{\theta}$ , is upward are again shown in purple and the regions where it is downward are shown in green. For the sake of this current qualitative argument, let the hemispheres be symmetric and consider that both the average age and the upwelling mass flux are known at the first level. Then, in the absence of mixing, the upwelling age on  $\theta_2$  is the sum of the age at  $\theta_1$  and the time it takes for air to traverse the distance from  $\theta_2 - \theta_1$ . If the air at  $\theta_2$  is any older, this additional age is due to the mixing between the upwelling and the downwelling regions. Because the upwelling mass flux can be determined by the difference between the upwelling and downwelling age, according to Equation 1, the mixing can thus be determined by knowledge of the vertical age gradient and the horizontal age difference. Figure 1c is identical to Figure 1b with the addition of orange arrows that represent the total mass flux into and out of the tropics due to this horizontal transport.

We develop the above qualitative arguments into a quantitative theory by considering the integration of the ideal age equation above an isotope in the tropical region to gain insight into the mixing between the tropics and extratropics. Here, “tropics” will be used to refer to the region where air is upwelling through an isentrope, and the “extratropics” where air is downwelling. Age is considered to be well-mixed within tropics and within the extratropics. As before, this is a steady-state derivation where the diabatic diffusion is negligible.

The ideal age equation (Waugh & Hall, 2002) states that the total derivative of age is equal to a source of 1 (year/year):

$$\frac{\partial \Gamma}{\partial t} + \mathcal{L}(\Gamma) = 1, \quad (5)$$

where  $\mathcal{L}$  is the advection–diffusion operator, with a boundary condition of zero age at the tropopause.

Because we are considering the statistically steady state, we neglect the time derivative. Integrating this equation over the total mass above the upwelling region of an isentrope (using the divergence theorem to address the bottom and extratropical boundaries) yields:

$$\int_{up} \mathbf{n} \cdot \mathbf{F}^\Gamma dA - \int \phi \sigma V_{in} \Gamma dl d\theta + \int \phi \sigma V_{out} \Gamma dl d\theta = \int_{V_{up}} \sigma dA d\theta. \quad (6)$$

$V_{in}$  and  $V_{out}$  are the integrated meridional velocity across the boundary between the upwelling and downwelling regions,  $\mathbf{n}$  is the vertical unit normal vector in isentropic coordinates, and  $\mathbf{F}^\Gamma$  is the mass-weighted age flux. Because diabatic diffusion is assumed to be negligible, the vertical transport is purely advective, and taking the vertical derivative in entropy results in

$$\frac{\partial}{\partial \theta} \int_{up} \sigma \dot{\theta} \Gamma dA - \phi \sigma V_{in} \Gamma dl + \phi \sigma V_{out} \Gamma dl = \int_{up} \sigma dA. \quad (7)$$

It is useful to define the entrainment and detrainment mass fluxes  $\mu_{in}$  and  $\mu_{out}$  (units of mass per unit theta per unit time) as follows:

$$\mu_{in} = \phi \sigma V_{in} dl, \quad (8)$$

and

$$\mu_{out} = \phi \sigma V_{out} dl. \quad (9)$$

The integral of the density will be indicated by  $\Sigma_u = \int_{up} \sigma dA$ . With these notation changes and simplifications, we can rewrite Equation 7 as:

$$\frac{\partial}{\partial \theta} \int_{up} \sigma \dot{\theta} \Gamma dA + \mu_{out} \Gamma_u - \mu_{in} \Gamma_d = \Sigma_u. \quad (10)$$

Then, the change in the diabatic circulation with entropy is due to the difference between the entrainment and detrainment mass fluxes:

$$\frac{\partial \mathcal{M}}{\partial \theta} = \mu_{in} - \mu_{out} = \frac{\partial}{\partial \theta} \int_{up} \sigma \dot{\theta} dA. \quad (11)$$

We rewrite Equation 10 in terms of  $\mathcal{M}$  and  $\Gamma_u$ :

$$\frac{\partial}{\partial \theta} \mathcal{M} \Gamma_u + \mu_{out} \Gamma_u - \mu_{in} \Gamma_d = \Sigma_u, \quad (12)$$

and with Equation 11, this becomes

$$\mathcal{M} \frac{\partial \Gamma_u}{\partial \theta} = \Sigma_u + \mu_{in} \Delta \Gamma. \quad (13)$$

The right hand side of this equation includes the two processes that determine the increase of age:  $\Sigma_u$ , which is the mass-weighted rate at which the air ages along the diabatic circulation, and  $\mu_{in} \Delta \Gamma$ , which is the rate at which adiabatic mixing between the tropics and extratropics increases the age of air. The mixing rate can be defined as  $\mu_{in}/\Sigma_u$ . Apart from  $\mu_{in}$ , all of the terms in Equation 13 can be easily diagnosed.

The equivalent extratropical expression is

$$-\mathcal{M} \frac{\partial \Gamma_d}{\partial \theta} = \Sigma_d - \mu_{out} \Delta \Gamma, \quad (14)$$

which can be derived in essentially the same way, and the derivation for the Southern Hemisphere extratropics is included as Appendix A.

We solve Equation 14 for the adiabatic rate of entrainment into the downwelling region:

$$\frac{\mu_{out}}{\Sigma_d} = \frac{\mathcal{M}}{\Sigma_d \Delta \Gamma} \frac{\partial \Gamma_d}{\partial \theta} + \frac{1}{\Delta \Gamma}, \quad (15)$$

and similarly express the adiabatic rate of entrainment into the upwelling region

$$\frac{\mu_{in}}{\Sigma_u} = \frac{\mathcal{M}}{\Sigma_u \Delta \Gamma} \frac{\partial \Gamma_u}{\partial \theta} - \frac{1}{\Delta \Gamma}. \quad (16)$$

The mixing rate derived in this way is closely related to previous work, such as that by Garny et al. (2014) or Neu and Plumb (1999). With the formulation of this theory in isentropic coordinates, the mean entrainment mass flux,  $\mu_{in}$ , is necessarily the adiabatic contribution, and our treatment has avoided the assumptions of constant mixing efficiency and vertical velocity with height. Mixing efficiency,  $\epsilon$ , was defined as the ratio of the entrainment mass flux into the tropics to the net detrainment mass flux into the extratropics by Neu and Plumb (1999) and has since been used frequently (e.g., Dietmüller et al., 2018; Ray et al., 2016). In our framework,  $\epsilon$  is height dependent and is given by the expression

$$\epsilon = \frac{\mu_{in}}{\mu_{out} - \mu_{in}} = \frac{\mu_{in}}{\partial \mathcal{M} / \partial \theta}. \quad (17)$$

Subject to caveats about mass-flux-weighting as opposed to area-weighting and the assumptions of hemispheric symmetry and a well-mixed extratropics, this enables a direct estimation of the adiabatic mixing from the age of air data. The steady-state assumption is necessary for this result to apply, however, and so long data records are required to perform this calculation.

## 2.2. Circulation in Each Hemisphere

Figure 1d shows schematically the separation of the two hemispheres with the adiabatic mixing in orange and the diabatic circulation shown in the purple and green arrows. The hemispheres are separated by a dynamical equator, which is the zero streamline of the steady state flow and need not be constant in the vertical. Using this zero streamline as the separation will ensure that there is no net mass flux from one hemisphere to the other, helping to make the hemispheres more like closed systems. The dash-dot lines show the separation between the upwelling and downwelling regions, corresponding to the zero of the diabatic velocity. These also can vary in the vertical. There is still an assumption related to hemispheric symmetry that is necessary, namely that the mass-flux-weighted age of upwelling air in the two different hemispheres is equal ( $\Gamma_{u_S} = \Gamma_{u_N}$ ) or close enough so that mixing across the zero streamline is negligible for the total age budget. This assumption is naturally met by the prior assumption of well-mixed tropics and is therefore not a more stringent requirement than in the global mean case. If that assumption is valid, any adiabatic mixing within the tropics will have no impact on the treatment of two separate hemispheres as closed systems. If the assumption is not valid, we could nevertheless make progress by considering the net age flux between the two hemispheres as a separate term in the age budget, and we are examining this in ongoing work.

If the hemispheres are closed systems, the theory described in Linz et al. (2016) and briefly revisited above can be applied separately to each hemisphere. We state some consequences of this application. The total diabatic mass flux through an isentropic surface is now separated into Northern Hemisphere mass flux,  $\mathcal{M}_N$ , and Southern Hemisphere mass flux,  $\mathcal{M}_S$ :

$$\mathcal{M} = \mathcal{M}_N + \mathcal{M}_S. \quad (18)$$

Similarly, the total mass above the isentropic surface in each hemisphere ( $M_N$  and  $M_S$ ) will be the total mass above the surface within the hemisphere, such that

$$M = M_N + M_S. \quad (19)$$

The age difference in each hemisphere is the difference between the mass-flux-weighted age of air downwelling through the isentrope in that hemisphere and the mass-flux-weighted age of upwelling air averaged between the  $\theta = 0$  line and the dynamic equator. Assuming no exchange between the two hemispheres or that the air exchanged in the tropics is of the same age, we have

$$\Delta\Gamma_S \mathcal{M}_S = M_S \quad (20)$$

and

$$\Delta\Gamma_N \mathcal{M}_N = M_N. \quad (21)$$

The derivation for the relationship between the mixing and the vertical gradient of age is nearly identical to the global tropical case considered above. In the Appendix A, we have performed this derivation for the Southern Hemisphere extratropics, and we state the results for the Southern Hemisphere tropics and extratropics here:

$$\mathcal{M}_S \frac{\partial\Gamma_{u_S}}{\partial\theta} = \Sigma_{u_S} + \mu_{in_S} \Delta\Gamma_S, \quad (22)$$

and

$$-\mathcal{M}_S \frac{\partial\Gamma_{d_S}}{\partial\theta} = \Sigma_{d_S} - \mu_{out_S} \Delta\Gamma_S. \quad (23)$$

These hold for the Northern Hemisphere as well. Thus, using the age distribution, the temperature, and the pressure, the mean entrainment and detrainment mass fluxes can be determined for both hemispheres. For this to be valid, the mixing of age across the dynamical equator should be negligible for the age budget. The dynamical equator can move with time, but integrating over long enough periods for the steady state assumption to be valid should cause the effect of this movement on the age transport to be small.

### 3. Model and Data Descriptions

Linz et al. (2016) tested the relationship between the diabatic circulation and the difference in upwelling and downwelling age of air on an isentrope using an idealized model with and without a seasonal cycle. We utilize a closely related idealized model setup here. The use of idealized models enables focus on the key resolved dynamical processes by not introducing any uncertainties on global circulation and transport related to physical parameterizations. Moreover, the use of idealized models alongside comprehensive ones provides a testbed to evaluate the theory in Section 2 in the absence of any explicit trends in circulation, which might be present in a freely evolving comprehensive model.

The study employs the FV3 finite volume dry dynamical core developed at the Geophysical Fluid Dynamics Laboratory (Putman & Lin, 2007). The core uses a cubed-sphere discretization in the horizontal and uses Lagrangian coordinates in the vertical. The model is integrated using a C48 cubed sphere horizontal grid, which corresponds to an effective horizontal resolution of  $2^\circ$ . In the vertical, 40  $\sigma - p$  hybrid levels are employed, of which 24 pure-pressure levels are located between the model top and 100 hPa. A similar setup, but devoid of a seasonal cycle, has also been previously employed by Gupta et al. (2020) to study the impact of numerics and resolution on the climatological age of air profile in the stratosphere.

We work with dry dynamics and do not include moisture or oceans. Diabatic heating in the troposphere and stratosphere, in the idealized model, is represented by Newtonian relaxation toward a slightly modified version of the analytical equilibrium temperature profiles proposed in Held and Suarez (1994) and Polvani and Kushner (2002), respectively. The modification implements a seasonally varying temperature profile in both the troposphere and stratosphere and is identical to the one proposed in Kushner and Polvani (2006). The vertical lapse rate parameter  $\gamma$  in the forcing, which determines the stratospheric polar vortex strength, is set to  $\gamma = -6$  K/km and the maximum hemispheric asymmetry parameter  $\epsilon$  is set to  $\epsilon = 10$  K. Seasonality in the tropospheric forcing is implemented by allowing the  $\epsilon$  parameter to oscillate between  $-10$  and  $10$  K annually. Similarly, in the stratosphere the equilibrium temperature at the poles annually oscillates between the vertically increasing US Standard Temperature (1976) profile and the uniform lapse rate ( $\gamma$ ) radiative cooling profile. The equilibrium temperature is further modified to raise the climatological tropopause in the model closer to the observed tropopause (Details of the modification are provided in Appendix B).

The southern hemisphere has no topography. To represent stronger planetary wave forcing in the Northern Hemisphere, a sinusoidal wave-2 topography as in Gerber and Polvani (2009) with a height amplitude of 4 km centered at  $45^\circ$  was imposed. The contrast in boundary wave forcing presents an extreme test for the hemispheric separation theory.

The age is computed by introducing a clock tracer near the surface (Hall & Plumb, 1994). In the source region, defined as  $p \geq 700$  hPa to be consistent with the height of the surface friction layer in Held and Suarez (1994), the clock tracer concentration  $\chi$  is specified to be  $\chi(\lambda, \phi, p, t) = t$  for  $p \geq 700$  hPa, where  $t$  is the model integration time,  $\lambda$  is the longitude, and  $\phi$  is the latitude. The model is run for 50 years, and the last 25 years are used for this analysis in order to ensure that the upper level age distribution has reached steady state.

Given the absence of so many physical processes in the idealized model; to better understand the application of both the age difference theory and the vertical age gradient theory developed above, we use a comprehensive global model. The model is the Community Earth System Model 1 Whole Atmosphere Community Climate Model (WACCM), an interactive chemistry-climate model (Garcia et al., 2017; Marsh et al., 2013). This model has the physical parameterizations and finite-volume dynamical core (Lin, 2004) from the Community Atmosphere Model, version 4 (Neale et al., 2013), and its domain extends from the surface to 140 km, with 31 pressure levels from 193 to 0.3 hPa. The horizontal resolution is  $2.5^\circ$  longitude by  $1.875^\circ$  latitude. The WACCM simulations are based on the Chemistry Climate Model Initiative REF-C1 scenario (Morgenstern et al., 2017). An ideal age tracer is included and is specified as in Garcia et al. (2011), with a uniform mixing ratio at the lower boundary that is linearly increasing in time. The model is forced with observed sea surface temperatures. The Quasi-Biennial Oscillation is nudged to observed winds, but otherwise the model evolves freely. The model run begins in 1979 and ends in 2014. Because this model run is clearly not in steady state, with at minimum a trend and substantial interannual variability in the

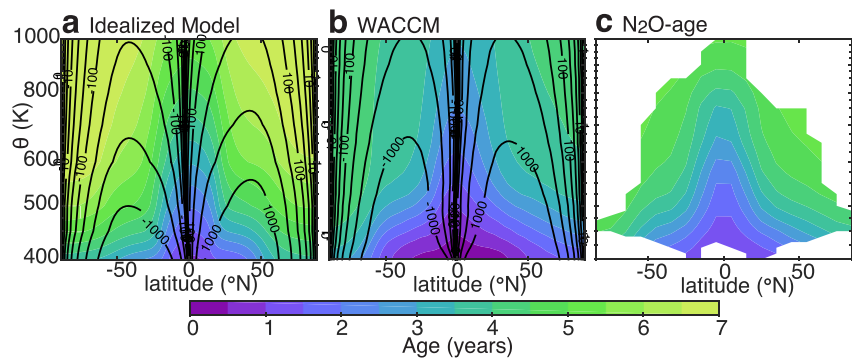


**Figure 2.** Zonal mean, time mean age of air shown in colors versus latitude and potential temperature for (a) the idealized model, (b) the Whole Atmosphere Community Climate Model (WACCM) model, and (c) the Global OZone Chemistry And Related trace gas Data records for the Stratosphere (GOZCARDS)  $N_2O$ -age product (Linz, 2017). Contours are spaced every 0.5 years. Also shown in (a) and (b) are the streamlines calculated based on the total diabatic circulation in  $kg\ m^{-1}s^{-1}$  with contours spaced logarithmically. White areas in (c) are places where sometimes the  $N_2O$  measurement is out of the range of the relationship between  $N_2O$  and age of air.

sea surface temperatures, we use this to test the steady-state assumption and to calculate the diagnostics described above.

The age data used in this paper (Linz, 2017) are a product created from the  $N_2O$  observations from the merged satellite data product Global OZone Chemistry And Related trace gas Data records for the Stratosphere (GOZCARDS) (Froidevaux et al., 2015). This is a combination of observations from the Microwave Limb Sounder (MLS) (Livesey et al., 2011), the Michelson Interferometer for Passive Atmospheric Sounding (MIPAS) (Fischer et al., 2008), and the Atmospheric Chemistry Experiment Fourier Transform Spectrometer (ACE-FTS, Bernath et al., 2005). MIPAS observations ceased in 2012. Long-lived tracers in the stratosphere have compact relationships (Plumb, 2002), and the particular relationship between  $N_2O$  and age of air was calculated from in situ data from campaigns in the 1990s (Andrews, Daube, et al., 2001). This empirical relationship was applied to calculate the age of air from the GOZCARDS  $N_2O$  for Linz et al. (2017), accounting for the trend in tropospheric  $N_2O$  (US Environmental Protection Agency, 2016). There are numerous uncertainties associated with this conversion, including but not limited to the potential non-stationarity of the relationship between  $N_2O$  and age of air and the expected meridional variation of the relationship (Plumb & Ko, 1992) that was neglected by Andrews, Daube, et al. (2001). Evidence for both of these being nonnegligible was found recently when B. Birner et al. (2020) updated the relationship between  $N_2$  and the age of air with in situ observations of stratospheric air measured by the tropospheric aircraft campaigns of the 2010s (Birner et al., 2020). This calculation showed distinct relationships in the Northern and Southern Hemisphere and possibly also disagreement with the Andrews, Daube, et al. (2001) relationship for older ages in the Northern Hemisphere. The data used by Birner et al. (2020) was taken somewhat incidentally during flights that were designed for primarily tropospheric characterization, and so they are limited in sampling locations and times when significant stratospheric intrusions were detected in the troposphere based on low water vapor and high ozone concentrations. These tended to be at quite high latitudes, making the Northern Hemisphere comparison with Andrews, Daube, et al. (2001) somewhat inappropriate. We proceed with the GOZCARDS  $N_2O$ -age calculated with the relationship from Andrews, Daube, et al. (2001), but we emphasize that the results from this calculation are not going to have a clearly defined error estimate.

To compare the mean state of these three products, consider Figure 2. This shows the zonal mean, time-mean age distribution for the  $N_2O$ -age and both models, and the streamfunctions for the models as well. Age is lowest in the tropics, where air is upwelling, and it is oldest at the poles, especially in the Southern Hemisphere. This hemispheric asymmetry at the poles is more pronounced in the realistic model than in the idealized model. The idealized model has significantly older ages and a weaker streamfunction than the comprehensive model. Note that for the idealized model, the air at 400 K is already 0.5 years old because of the weak tropospheric circulation and the reference of age to the 700 hPa level. The comprehensive model is also younger than the  $N_2O$ -age by about a year. The shape of the isopleths beneath 550 K is quite similar,

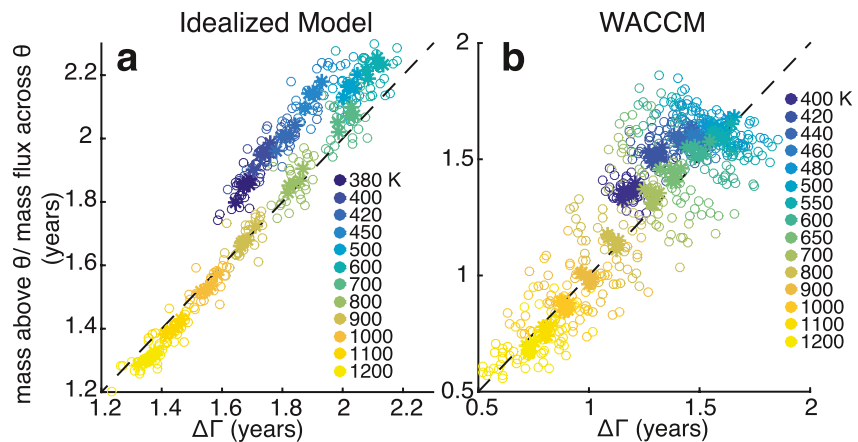


**Figure 3.** Scatter plots of the ratio of mass above each isentropic surface to the mass flux through the isentropic surface against the difference in mass-flux-weighted age of downwelling and upwelling air through that surface for (a) the idealized model and (b) the Whole Atmosphere Community Climate Model (WACCM) model. One-year averages are shown in the empty circles and five-year averages are shown in the stars. The relationship predicted by the theory of Linz et al. (2016) is shown in the black dashed one-to-one line. Different colors show different isentropic levels in K.

and above that level, the  $N_2O$ -age has shallower slopes from the tropics to the midlatitudes. This will be discussed again in Section 5.

## 4. Applying the Theory in an Idealized and a Realistic Model

### 4.1. Time Dependence

The steady-state assumption means that this theory is not applicable to high-frequency variability, and so we investigate the timescale over which averaging must be performed for the theory to be useful. We test to see how well the steady-state age difference theory in Equation 1 holds in these two models with different lengths of averaging. An example of such a comparison is shown in Figure 3, where the ratio of the mass above each isentropic surface to the mass flux through that surface is plotted against the mass-flux-weighted age of air difference between downwelling and upwelling air through each isentropic surface. Averages using one year are shown in the empty circles, and averages over five years are shown in the stars. Note that the averaging is performed after the division. The points are colored according to the isentropic level, with the navy points in the lower stratosphere and yellow points in the upper stratosphere. The one-to-one line predicted by Equation 1 is shown in the dashed black line. For the idealized model (left panel), one-year averages cluster together relatively closely, but the five-year averages show a reduced spread. For the comprehensive WACCM model (right panel), the one-year averages show dramatically more spread than the variability captured by the idealized model suggesting a more important role for the time-dependent terms, but the variability between five-year averages is quite small. Calculations of the magnitude of the time-dependent terms show that with this averaging length, they are negligible (not shown, see Linz et al., 2016 for details of time-dependent terms). At the lower levels, the points fall above the one-to-one line predicted by the theory, which is consistent with stronger diabatic diffusion in the lowermost stratosphere (Sparling et al., 1997). In both models, there is a local maximum in the age difference at around 500–550 K, which indicates a relative minimum in the velocities. In the upper levels, the points fall on the line. At the uppermost levels, the points fall slightly below the line, which is unexplained (and physically inconsistent). This discrepancy can be amplified with a different choice of time-averaging (i.e., by averaging in time before performing the division). This small effect could be an indication of imperfections associated with performing the calculations on isentropic levels after interpolation as opposed to performing the calculations on model levels and then interpolating to isentropes. It could also be the result of unrealistic numerical diffusion (c.f., Gupta et al., 2020).

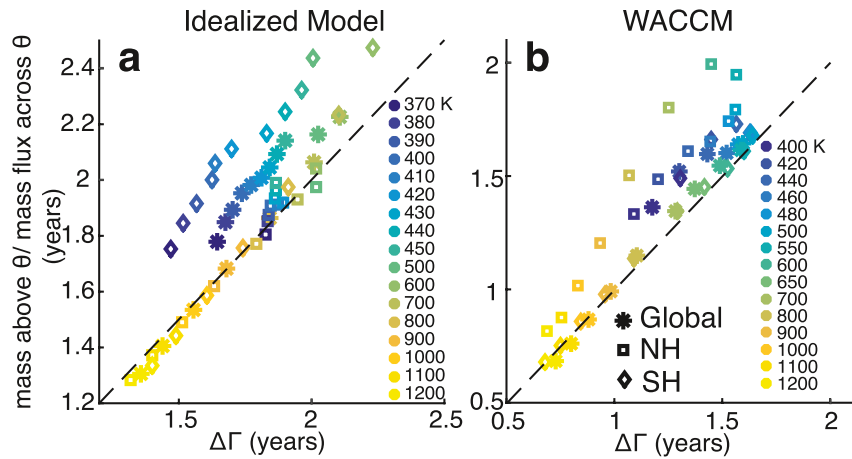


**Figure 4.** As in Figure 3, except now averaged over the entire period (as specified in Section 3). Global means are shown in the stars, and the Northern Hemisphere and Southern Hemisphere, separated according to the theory in Section 2.2, are shown in squares and diamonds, respectively. Colors again show the isentropic levels. The one-to-one line of the theory is the dashed line.

#### 4.2. Separating Hemispheres

As discussed in the introduction, the circulation in the Southern Hemisphere is expected to evolve in time differently from that in the Northern Hemisphere.

When we separate the two hemispheres according to the theory in Section 2.2, we assume that the exchange of tropical air across the equator associated with the seasonal cycle and other time variation has negligible impact on the total age budget for each hemisphere, allowing the hemispheres to be treated as two independent systems. To see whether this assumption is reasonable, we can once more test the validity of Equation 1 and see whether this separation of the two hemispheres has made the agreement with the theory worse. If, for example, the Southern Hemisphere tropical air were younger and mixed substantially into the Northern Hemisphere, then age difference in the Northern Hemisphere would be larger than predicted by the theory, and points for the Northern Hemisphere would tend to fall below the one-to-one theory line. Figure 4 is the same type of scatter plot as in Figure 3 but now averaged over the entire time period and showing different hemispheres in the different symbols. In the idealized model (left panel), the Southern Hemisphere (diamonds) has a substantially reduced age difference than the global mean age difference (stars), but the ratio of the mass to the mass flux does not decrease accordingly. Meanwhile, the agreement with a theory from the Northern Hemisphere (squares) is better than the global agreement. The implication is that in the lower stratosphere, there is some exchange of air that is not of the same age, increasing the Northern Hemisphere age difference and decreasing the Southern Hemisphere age difference. Above about 800 K, the two hemispheres agree as well with the theory as the global average. For the WACCM model (right panel), the Northern and Southern Hemispheres both agree as well with the theory as the global up to about 500 K, at which point the Northern Hemisphere agreement breaks down. Although both models have problematic regions, we proceed to calculate the mixing diagnostics as an example.

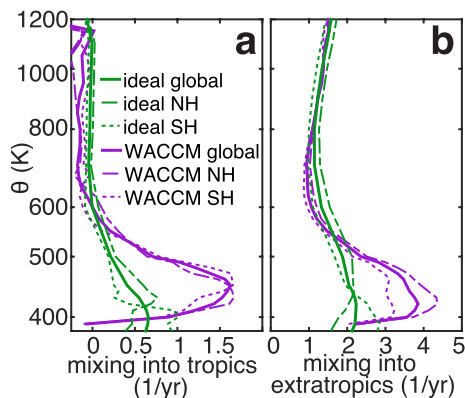


**Figure 5.** Mixing rate into ( $\mu_{in}/\Sigma_u$ , (a)) and out of ( $\mu_{out}/\Sigma_d$ , (b)) the tropics for the idealized model (green) and the Whole Atmosphere Community Climate Model (WACCM) model (purple) versus potential temperature. Global averages are in the solid lines, while the Northern Hemisphere averages are in the dash-dot lines and the Southern Hemisphere averages are in the dotted lines.

With the caveat that there are regions where the hemispheric independence breaks down, we can still examine the separation between the hemispheres and the overall mixing rates. The mixing rates into and out of the tropics for the two models and their separate hemispheres are shown in Figure 5. The WACCM model separation is mostly reliable below 500 K, and in this region, we see that mixing into the tropics peaks on a higher isentropic level in the Southern Hemisphere than in the Northern

Hemisphere. The mixing out of the tropics in the Northern Hemisphere peaks at the same level as the mixing into the tropics, but this mixing is much stronger than in the Southern Hemisphere. This asymmetry may be due to the monsoonal circulation (Vogel et al., 2019). In the idealized model, we expect Northern Hemisphere mixing to be larger than Southern Hemisphere mixing, as there is no zonally asymmetric forcing applied in the Southern Hemisphere. Where the results can be relied on, that is, above about 700 K, this is certainly the case.

For the global average mixing rates, we see that almost no air is mixed into the tropics above 600 K in either model. Mixing into the extratropics has a local minimum for both models at 600 K, which is above the local minimum in the relative diabatic velocities at 500–550 K (this minimum can be seen as the maximum value of the age difference in Figure 3). If wave breaking is driving both the adiabatic mixing at a given level and the diabatic circulation at that level and below, this distribution of mixing is consistent. For both models, there is some mixing into the extratropics above about 800 K, implying an increase in wave breaking there. The idealized model's much weaker mixing would lead to an overall younger age than WACCM, but its diabatic circulation is also much weaker (see streamfunctions in Figure 2), consistent with the older ages in the idealized model. In Figure 4, the mixing into the tropics for the WACCM model hovers just below zero above 700 K and around 380 K. This is not an issue with the mechanics of the calculation, but instead implies that the assumptions about the uniformity of the age of air within the upwelling and downwelling regions are (unsurprisingly) flawed. Such weakly negative mixing flux above 600 K were also obtained by Gupta et al. (2021) who used the isentropic framework proposed in this study to estimate the mixing flux into the tropics in idealized models, but for a perpetual winter solstice climatology. Strong horizontal gradients of age in the upwelling and downwelling regions in their models led to an overestimation of the mixed age difference  $\Delta\Gamma$  resulting in the underestimation of mixing fluxes. Additional examination to quantify this bias is warranted in future work. The global results are qualitatively similar to the global results from Ray et al. (2016) for the Canadian Middle Atmosphere Model, although quantitative comparisons are difficult because of the different coordinate system and assumptions in that study. The results can also be qualitatively compared with the equivalent length calculations done in reanalyses by Abalos et al. (2016), which showed maximum mixing at around 450 K in both hemispheres, with higher equivalent lengths in the Northern Hemisphere than the Southern Hemisphere up to about 500 K (where the WACCM hemispheric separation is valid). A more comprehensive and quantitative comparison of different mixing metrics is underway.

## 5. Comparison With N<sub>2</sub>O-Age

One of the most potentially powerful applications of this theory is the ability to use observations to compare more directly to models—to compare like-to-like with simple, global metrics. Although there are numerous caveats about the current observational global age of air products that are available and about the age of air from N<sub>2</sub>O in particular, we nevertheless think it is a valuable demonstration to apply the theory to a satellite record. We are demonstrating the method, but we will not calculate the error bars, as we currently cannot determine what should even be included in such a calculation. An incomplete list includes: the bias introduced by using area-weighting instead of mass flux weighting, uncertainty due to reanalysis choice for calculating pressure levels and pressure-to-isentrope conversion, uncertainty in the calculation of the CO<sub>2</sub> lag time, uncertainty in the relationship between N<sub>2</sub>O and CO<sub>2</sub> lag time (in particular, the use of a relationship from data that is over a decade older than the satellite record's beginning date), the use of a relationship that has been defined primarily by Northern Hemisphere midlatitude in situ data to characterize global age of air (Andrews, Daube, et al., 2001) (even though the tropical and extratropical relationships should differ, e.g., Plumb, 2007), uncertainty in vertical gradients introduced by satellite weighting functions, and uncertainty due to the nonuniformity of age within the tropics and within the extratropics. As such, these calculations should be taken as only a first guess.

Because of the limited extent of the relationship between N<sub>2</sub>O and CO<sub>2</sub> lag time, the vertical extent of age coverage is much greater in the tropics than in the extratropics (see Figure 2). We therefore calculate the vertical age gradient in the tropics, and this is a more reliable metric than the other global metrics. It is not, however, a complete characterization of the mixing (c.f., Equation 13), since the total overturning strength and horizontal age gradients are also important. In Figure 6, we find a remarkable agreement in

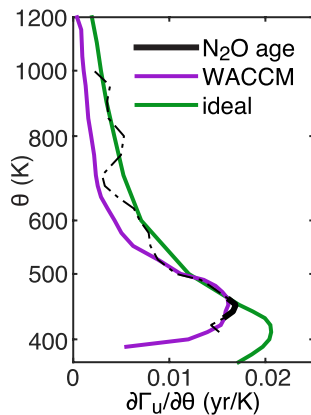


**Figure 6.** The vertical gradient of the mean upwelling age of air (mass flux weighted for models, area-weighted for  $N_2O$ -age) for the ideal model (green), Whole Atmosphere Community Climate Model (WACCM) model (purple), and for the  $N_2O$ -age (black). The only levels for which the data record is complete are shown in the thick black line, while the dash-dot black line shows the mean vertical age gradient while ignoring the data gaps. There are far fewer gaps in the tropics than in the extratropics, so this is more reliable than the age difference shown later.

Finally, we look at the two primary summary statistics: the overturning circulation strength and the mixing efficiency,  $\epsilon$ . These require the full global data coverage, and so we calculate these wherever we have any data, even if the temporal coverage is incomplete. The levels where we have global observational age data for the entire length of the record are shown in the thick, solid black lines in Figure 7. The comparison of the total overturning, based on the horizontal age gradient, is shown in Figure 7a, and the idealized model is shown to have significantly weaker circulation. The WACCM model agrees fairly closely with the  $N_2O$ -age calculation. The mixing efficiency is shown in Figure 7b, and here too, there is an agreement between the WACCM model and the  $N_2O$ -age calculation, where full satellite data exist. Higher up, the mixing efficiency implied by the  $N_2O$  is much greater than that in both of the models, but we caution that the extratropical data are very limited there. The missing data are not uniform in time; the oldest ages are missing, and so the age will have a height-dependent low bias in the downwelling regions. The idealized model has a lower mixing efficiency, consistent with what we saw previously in Figure 4. This global model-to-model comparison is also a particularly useful application of this theory, as these are well-defined metrics describing the global stratospheric circulation.

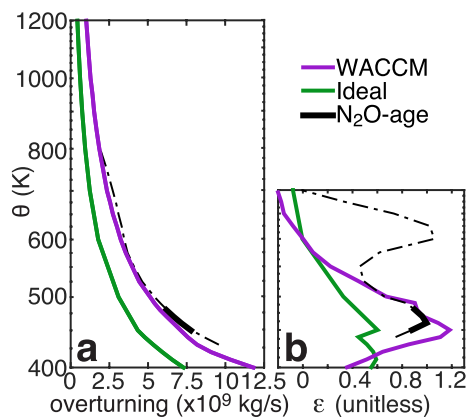


**Figure 7.** Summary statistics for both models and for the  $N_2O$ -age product. Mixing rate into and out of the tropics for the two hemispheres and the global average for Whole Atmosphere Community Climate Model (WACCM).

the vertical age difference in the tropics between WACCM and the  $N_2O$ -age where the full data exist, and the idealized model also agrees reasonably well between 480 and 500 K. Higher up, the vertical age gradient is larger in the idealized model than in the WACCM model. All three profiles show a peak in the lower stratosphere (lower in the idealized model than in WACCM and the  $N_2O$ -age) associated with a peak in the mixing into the tropics at that level. Agreement in the vertical gradient of age in the tropics only implies agreement in mixing if there is also agreement in the overturning, but the quantitative similarity between the vertical age gradient in the tropics between WACCM model and the  $N_2O$ -age is remarkable. Although the age gradients in WACCM are very similar to those in the  $N_2O$ -age product below 550 K, the absolute magnitude of age is significantly lower. This is likely due to a discrepancy at the point of entry into the stratosphere, where the  $N_2O$ -age product does not exist.

Finally, we look at the two primary summary statistics: the overturning circulation strength and the mixing efficiency,  $\epsilon$ . These require the full global data coverage, and so we calculate these wherever we have any data, even if the temporal coverage is incomplete. The levels where we have global observational age data for the entire length of the record are shown in the thick, solid black lines in Figure 7. The comparison of the total overturning, based on the horizontal age gradient, is shown in Figure 7a, and the idealized model is shown to have significantly weaker

## 6. Discussion and Conclusions

We have derived a method to calculate a diagnostic for the mixing rate between the tropics and extratropics from the spatial gradients of age of air, in steady state and assuming diabatic diffusion is small. By formulating the theory based on the TLP framework of Neu and Plumb (1999) on isentropic levels, we allow for both the diabatic velocities and the mixing efficiency to vary in the vertical. The vertical gradient of age in the extratropics informs the mean detrainment rate out of the tropics, and the vertical gradient of age of air in the tropics informs the mean entrainment rate into the tropics. Taking advantage of the theory of Linz et al. (2016), we can use the quasi-horizontal difference of downwelling and upwelling age of air to calculate the diabatic circulation strength. With observations of age, temperature, and pressure, we can calculate both a tropical entrainment and detrainment mass flux. Stratospheric age of air alone is sufficient to quantitatively determine the circulation as defined by these global or hemispheric averages in steady state. We note that unlike the theory of Linz et al. (2016), the mixing metric is a diagnostic tool that reflects the assumptions we have made about the system (for example, that the average age that mixes from the extratropics into the tropics is the mass-flux-weighted mean age of downwelling air). However, these assumptions are necessary to develop the theory to relate the age of air

observations to the adiabatic mixing, and we believe this will prove to be useful to compare model runs with an age tracer to stratospheric age observations.

This method is limited because of the steady-state assumption. Linz et al. (2016) showed that in an idealized model, annual averages were generally sufficient for the steady-state assumption to hold for the relationship between the diabatic circulation strength and the age difference between downwelling and upwelling air. Linz et al. (2017) used five-year averages of two data products to calculate the mean circulation strength and implicitly demonstrate that these five-year averages are good enough using a realistic model. Here, we more systematically examine that treatment and find that a five-year average is indeed sufficient. Because mixing timescales tend to be shorter than the diabatic circulation timescales, it seems likely that the minimum period of averaging for the steady-state assumption to apply would be limited by the diabatic component. However, this is not straightforward to test—a comparison to the more traditional effective diffusivity analysis in a realistic model would be a first step. The steady-state assumption also necessarily makes this theory inappropriate for examining short-term changes to the circulation. Instead, it is more appropriate for characterizing and comparing model mean adiabatic mixing to the mean adiabatic mixing of the true atmosphere and the decadal variations in these.

Many stratospheric processes, such as ozone depletion and recovery, affect the hemispheres asymmetricaly, and so the global-average picture is useful, but incomplete. We derived the relationships for the hemispheres separately; however, to do so, we assumed that the two hemispheres act as independent closed systems, which is not reasonable. This is only true if the air that is exchanged across the equator is of approximately the same age, and so the assumption introduces errors. For quantitative use, the errors introduced would need further examination, and the exchange could be included in the budget explicitly in a slightly more complex formulation of the theory. In the WACCM model, the assumption of hemispheric independence appears to be reasonable up to about 500 K, and there is more mixing in the Northern Hemisphere than the Southern Hemisphere. In the idealized run, the assumption holds for the middle to upper stratosphere, and although mixing is weak, the Northern hemisphere has more mixing than the Southern hemisphere, consistent with the stronger forcing. The current theory does not provide information about where in the longitude the mixing is concentrated, though a framework with zonal asymmetry could be developed. These mixing rates were consistent with what could be expected based on the different forcing in the Northern and Southern Hemispheres, and so we conclude that this approach might be viable, though it would be more useful with an explicit treatment of interhemispheric transport. Globally, we find a relative minimum in mixing around 600 K and complete isolation of the tropics above this level.

This theory holds potential to enable calculations of the mean adiabatic mixing of the real stratosphere from age of air observations. Although no reliable global mean age observations exist, work is being done to combine a number of satellite data products (including CH<sub>4</sub>, N<sub>2</sub>O, and SF<sub>6</sub>) to create a climatology of stratospheric age of air. We have performed an example calculation using N<sub>2</sub>O satellite observations combined with in situ observations. We discussed many limitations in Section 5, but we highlight a few here: the uncertainty in the determination of age from N<sub>2</sub>O for numerous reasons, the vertical resolution and sampling pattern of the satellite, and the effect of area-weighting rather than mass-flux weighting. Before we have reliable mixing estimates from satellites, these uncertainties and others must be addressed. However, this is a promising first step, and the comprehensive WACCM model agrees remarkably well with the mixing estimates from the N<sub>2</sub>O-age in the regions where data coverage is substantial. The quantification of the stratospheric circulation from observations in a way that enables meaningful comparisons with models is an important topic of study, and this theory provides a significant step forward toward that goal.

## Appendix A

For the derivation of the Southern Hemisphere extratropical mixing rate, start again with the ideal age equation (Waugh & Hall, 2002):

$$\frac{\partial \Gamma}{\partial t} + \mathcal{L}(\Gamma) = 1. \quad (\text{A1})$$

As before, we assume that diabatic diffusion is negligible and make the assumption of steady-state flow. Then, we integrate this equation over the volume above the Southern Hemisphere downwelling region on an isentrope:

$$\int_{S_{down}} \mathbf{n} \cdot \mathbf{F}^\Gamma dA - \int \oint \sigma V_{in} \Gamma dl d\theta + \int \oint \sigma V_{out} \Gamma dl d\theta = \int_{S_{down}} \sigma dA d\theta. \quad (\text{A2})$$

$dl$  is now only over the one surface that divides the Southern extratropics from the tropics, the Southern  $\dot{\theta} = 0$  line. Then take the vertical derivative in entropy to obtain

$$\frac{\partial}{\partial \theta} \int_{S_{down}} \sigma \dot{\theta} \Gamma dA - \oint \sigma V_{in} \Gamma dl + \oint \sigma V_{out} \Gamma dl = \int_{S_{down}} \sigma dA. \quad (\text{A3})$$

c.f., Equation A7. The air coming into the extratropics is assumed to have the mass-flux-weighted average age of the tropical region ( $\Gamma_{u_S}$ ), and likewise the air leaving the extratropics has the mass-flux-weighted average age of the Southern extratropical region ( $\Gamma_{d_S}$ ). Define the entrainment and detrainment mass fluxes  $\mu_{in_S}$  and  $\mu_{out_S}$ :

$$\mu_{in_S} = \oint \sigma V_{in} dl, \quad (\text{A4})$$

and

$$\mu_{out_S} = \oint \sigma V_{out} dl, \quad (\text{A5})$$

recalling that the line integral is now only across the Southern Hemisphere surface between the tropics and extratropics. Then rewrite the integral of the density as  $\Sigma_{d_S} = \int_{S_{down}} \sigma dA$ . With these notation changes and simplifications, we can rewrite Equation A3 as:

$$\frac{\partial}{\partial \theta} \int_{S_{up}} \sigma \dot{\theta} \Gamma dA - \mu_{out_S} \Gamma_{u_S} + \mu_{in_S} \Gamma_{d_S} = \Sigma_{d_S}. \quad (\text{A6})$$

As globally the change in the Southern Hemisphere diabatic circulation with entropy is due to the difference between the entrainment and detrainment mass fluxes:

$$\frac{\partial \mathcal{M}_S}{\partial \theta} = \mu_{in_S} - \mu_{out_S} = \frac{\partial}{\partial \theta} \int_{S_{up}} \sigma \dot{\theta} dA = -\frac{\partial}{\partial \theta} \int_{S_{down}} \sigma \dot{\theta}. \quad (\text{A7})$$

We rewrite Equation A6 in terms of  $\mathcal{M}_S$  and  $\Gamma_{d_S}$ :

$$-\frac{\partial}{\partial \theta} \mathcal{M}_S \Gamma_{d_S} - \mu_{out_S} \Gamma_{u_S} + \mu_{in_S} \Gamma_{d_S} = \Sigma_{d_S}, \quad (\text{A8})$$

## Appendix B

Diabatic heating in the idealized model is provided through Newtonian relaxation of the model atmosphere temperature toward an analytical equilibrium temperature profile  $T_{eq}$ . The equilibrium temperature profile in the Polvani-Kushner stratosphere is computed using the U.S. 1976 Standard Atmosphere profile (from rocketsondes and satellite data). This profile records the vertical variation of atmospheric temperature and pressure at eight different atmospheric heights between the surface and 71 km. The tropopause height in the idealized model is adjusted by modifying  $T_{eq}$  in the upper troposphere lower stratosphere (UTLS) region by adjusting the U.S. 1976 Standard Atmosphere profile.

The profile is piecewise linear that is, the temperature is assumed to vary linearly between each of the eight points with a fixed lapse rate in the region. For the first two levels near the surface, the temperature steadily decreases at a lapse rate of  $-6.5$  K/km, decreasing from 288.15 to 216.65 K between 1,000 and 223.36 hPa, respectively. In the UTLS, the levels 223.36 and 54 hPa are isothermal with a temperature of 216.65 K. In the middle stratosphere, between 54 and 8.5 hPa, the temperature increases again at a constant rate from 216.65 to 228.6 K, respectively.

The tropopause height in the idealized model employed in the study is raised by lowering the equilibrium temperature in the UTLS from its default value of 216.65 K to a new forcing temperature of 200 K. The static stability (lapse rate) between 1,000 and 223.36 hPa and between 223.36 and 54 hPa is kept unchanged at  $-6.5$  and  $0$  K/km, respectively. As a result, the 200 K forcing temperature is associated with a pressure height of roughly 150 hPa and therefore, the isothermal UTLS region is now relaxed toward an equilibrium temperature of 200 K instead of 216.5 K. Any forcing temperature less than 216.65 K raises the tropopause height; and the forcing temperature of 200 K raises the climatological tropical tropopause in the model roughly from 200 hPa ( $\sim 12$  km) to 140 hPa ( $\sim 14$  km).

## Data Availability Statement

The age of the air data product is the same as that used in Linz et al. (2017) and is available here: <https://doi.org/10.6084/m9.figshare.5229844.v1>. The model data are available here: <https://doi.org/10.7910/DVN/GBRCWW> (Linz, 2021). The authors have consulted with the JGR-Atmospheres editorial staff and editor in chief about these circumstances prior to submission.

## Acknowledgments

First, the authors would like to thank Douglas E. Kinnison for providing the WACCM data for this study. WACCM is a component of the Community Earth System Model (CESM), which is supported by the National Science Foundation (NSF) and the Office of Science of the U.S. Department of Energy. Computing resources were provided by NCAR's Climate Simulation Laboratory, sponsored by NSF and other agencies. This research was enabled by the computational and storage resources of NCAR's Computational and Information System Laboratory (CISL). We would also like to thank our very helpful reviewers. This research was conducted with Government support for M. Linz under and awarded by DoD, Air Force Office of Scientific Research, National Defense Science and Engineering Graduate (NDSEG) Fellowship, 32 CFR 168a. M. Linz was also partially supported by the NSF award AGS-1608775. This work was also supported in part by the National Science Foundation grants AGS-1547733 to MIT and AGS-1546585 and AGS-1852727 to NYU.

## References

- Abalos, M., Legras, B., & Shuckburgh, E. (2016). Interannual variability in effective diffusivity in the upper troposphere/lower stratosphere from reanalysis data. *Quarterly Journal of the Royal Meteorological Society*, *142*(697), 1847–1861. <https://doi.org/10.1002/qj.2779>
- Allen, D. R., & Nakamura, N. (2001). A seasonal climatology of effective diffusivity in the stratosphere. *Journal of Geophysical Research*, *106*(D8), 7917–7935. <https://doi.org/10.1029/2000JD900717>
- Andrews, A. E., Boering, K. A., Daube, B. C., Wofsy, S. C., Hints, E. J., & Weinstock, E. M. (1999). Empirical age spectra for the lower tropical stratosphere from in situ observations of CO<sub>2</sub>: Implications for stratospheric transport TM. *Journal of Geophysical Research*, *104*(D21), 26581–26595.
- Andrews, A. E., Boering, K. A., Wofsy, S. C., Daube, B. C., Jones, D. B., Alex, S., et al. (2001). Empirical age spectra for the midlatitude lower stratosphere from in situ observations of CO<sub>2</sub>: Quantitative evidence for a subtropical “barrier” to horizontal transport. *Journal of Geophysical Research*, *106*.
- Andrews, A. E., Daube, B. C., Wofsy, S. C., Loewenstein, M., Jost, H., Podolske, J. R., et al. (2001). Mean ages of stratospheric air derived from in situ observations of CO, CH<sub>4</sub>, and N<sub>2</sub>O. *Journal of Geophysical Research*, *106*.
- Andrews, D. G., & McIntyre, M. F. (1976). Planetary waves in horizontal and vertical shear: Asymptotic theory for equatorial waves in weak shear. *Journal of the Atmospheric Sciences*, *33*(11), 20492–2053. [https://doi.org/10.1175/1520-0469\(1976\)033h2049:PWIHAVi2.0.CO;2](https://doi.org/10.1175/1520-0469(1976)033h2049:PWIHAVi2.0.CO;2)
- Bernath, P. F., McElroy, C. T., Abrams, M. C., Boone, C. D., Butler, M., Camy-Peyret, C., et al. (2005). Atmospheric chemistry experiment (ace): Mission overview. *Geophysical Research Letters*, *32*(15). <https://doi.org/10.1029/2005GL022386>
- Birner, B., Chipperfield, M. P., Morgan, E. J., Stephens, B. B., Linz, M., Feng, W., et al. (2020). Gravitational separation of Ar/N<sub>2</sub> and age of air in the lowermost stratosphere in airborne observations and a chemical transport model. *Atmospheric Chemistry and Physics*, *20*(21), 12391–12408. <https://doi.org/10.5194/acp-20-12391-2020>
- Birner, T., & Bönisch, H. (2011). Residual circulation trajectories and transit times into the extratropical lowermost stratosphere. *Atmospheric Chemistry and Physics*, *11*(2), 817–827. <https://doi.org/10.5194/acp-11-817-2011>
- Boering, K. A., Wofsy, S. C., Daube, B. C., Schneider, H. R., Loewenstein, M., Podolske, J. R., & Conway, T. J. (1996). Stratospheric mean ages and transport rates from observations of carbon dioxide and nitrous oxide. *Science*.
- Brewer, A. W. (1949). Evidence for a world circulation provided by measurements of helium and water vapour distribution in the stratosphere. *Quarterly Journal of the Royal Meteorological Society*, *75*, 351–363. <https://doi.org/10.1002/qj.49707532603>
- Butchart, N. (2014). The Brewer–Dobson circulation. *Reviews of Geophysics*, *52*, 157–184. <https://doi.org/10.1002/2013RG000448>
- Butchart, N., Scaife, a. a., Bourqui, M., Grandpré, J., Hare, S. H. E., Kettleborough, J., et al. (2006). Simulations of anthropogenic change in the strength of the Brewer–Dobson circulation. *Climate Dynamics*, *27*(7–8), 727–741. <https://doi.org/10.1007/s00382-006-0162-4>
- Dietmüller, S., Eichinger, R., Garny, H., Birner, T., Boenisch, H., Pitari, G., et al. (2018). Quantifying the effect of mixing on the mean age of air in ccmval-2 and ccmi-1 models. *Atmospheric Chemistry and Physics*, *18*(9), 6699–6720. <https://doi.org/10.5194/acp-18-6699-2018>
- Dobson, G. M. B., Harrison, D. N., & Lawrence, J. (1929). Measurements of the amount of ozone in the Earth's atmosphere and its relation to other geophysical conditions. *Proceedings of the Royal Society A*, *122*, 456–486.
- Ehhalt, D. H., Rohrer, F., Blake, D. R., Kinnison, D. E., & Konopka, P. (2007). On the use of nonmethane hydrocarbons for the determination of age spectra in the lower stratosphere. *Journal of Geophysical Research*, *112*(D12), D12208. <https://doi.org/10.1029/2006JD007686>
- Fischer, H., Birk, M., Blom, C., Carli, B., Carlotti, M., von Clarmann, T., et al. (2008). Mipas: An instrument for atmospheric and climate research. *Atmospheric Chemistry and Physics*, *8*(8), 2151–2188. <https://doi.org/10.5194/acp-8-2151-2008>
- Fritsch, F., Garny, H., Engel, A., Bönisch, H., & Eichinger, R. (2020). Sensitivity of age of air trends to the derivation method for non-linear increasing inert sf<sub>6</sub>. *Atmospheric Chemistry and Physics*, *20*(14), 8709–8725. <https://doi.org/10.5194/acp-20-8709-2020>
- Froidevaux, L., Anderson, J., Wang, H.-J., Fuller, R. A., Schwartz, M. J., Santee, M. L., et al. (2015). Global ozone chemistry and related trace gas data records for the stratosphere (gozcards): Methodology and sample results with a focus on hcl, H<sub>2</sub>O, and O<sub>3</sub>. *Atmospheric Chemistry and Physics*, *15*(18), 10471–10507. <https://doi.org/10.5194/acp-15-10471-2015>
- Fu, Q., Lin, P., Solomon, S., & Hartmann, D. L. (2015). Observational evidence of strengthening of the Brewer–Dobson circulation since 1980. *Journal of Geophysical Research*, *120*, 10214–10228. <https://doi.org/10.1002/2015JD023657>
- Garcia, R. R., & Randel, W. J. (2008). Acceleration of the Brewer–Dobson circulation due to increases in greenhouse gases. *Journal of the Atmospheric Sciences*, *65*(8), 2731–2739. <https://doi.org/10.1175/2008JAS2712.1>
- Garcia, R. R., Randel, W. J., & Kinnison, D. E. (2011). On the determination of age of air trends from atmospheric trace species. *Journal of the Atmospheric Sciences*, *68*(1), 139–154. <https://doi.org/10.1175/2010JAS527.1>

- Garcia, R. R., Smith, A. K., Kinnison, D. E., de la Camara, A., & Murphy, D. J. (2017). Modification of the gravity wave parameterization in the whole atmosphere community climate model: Motivation and results. *Journal of the Atmospheric Sciences*, 74(1), 275–291. <https://doi.org/10.1175/JAS-D-16-0104.1>
- Garny, H., Birner, T., Boenisch, H., & Bunzel, F. (2014). The effects of mixing on age of air. *Journal of Geophysical Research*, 119, 7015–7034. <https://doi.org/10.1002/2013JD021417>
- Gerber, E. P., & Polvani, L. M. (2009). Stratosphere–troposphere coupling in a relatively simple AGCM: The importance of stratospheric variability. *Journal of Climate*, 22(8), 1920–1933. <https://doi.org/10.1175/2008JCLI2548.1>
- Glanville, A. A., & Birner, T. (2017). Role of vertical and horizontal mixing in the tape recorder signal near the tropical tropopause. *Atmospheric Chemistry and Physics*, 17(6), 4337–4353. <https://doi.org/10.5194/acp-17-4337-2017>
- Gupta, A., Gerber, E. P., & Lauritzen, P. H. (2020). Numerical impacts on tracer transport: A proposed intercomparison test of atmospheric general circulation models. *Quarterly Journal of the Royal Meteorological Society*, 146(733), 3937–3964. <https://doi.org/10.1002/qj.3881>
- Gupta, A., Gerber, E. P., Plumb, R. A., & Lauritzen, P. H. (2021). Numerical impacts on tracer transport: Diagnosing the influence of dynamical core formulation and resolution on stratospheric transport. *Journal of the Atmospheric Sciences*. <https://doi.org/10.1175/JAS-D-21-0085.1>
- Hall, T. M., & Plumb, R. A. (1994). Age as a diagnostic of stratospheric transport. *Journal of Geophysical Research*, 99(D1), 1059–1070. <https://doi.org/10.1029/93JD03192>
- Hauck, M., Fritsch, F., Garny, H., & Engel, A. (2019). Deriving stratospheric age of air spectra using an idealized set of chemically active trace gases. *Atmospheric Chemistry and Physics*, 19(7), 5269–5291. <https://doi.org/10.5194/acp-19-5269-2019>
- Haynes, P., & Shuckburgh, E. (2000). Effective diffusivity as a diagnostic of atmospheric transport 1. Stratosphere. *Journal of Geophysical Research*, 105, 777–794.
- Held, I. M., & Suarez, M. J. (1994). A proposal for the intercomparison of the dynamical cores of atmospheric general circulation models. *Bulletin of the American Meteorological Society*, 75, 1825–1830. [https://doi.org/10.1175/1520-0477\(1994\)075<1825:APFTIOI>2.0.CO;2](https://doi.org/10.1175/1520-0477(1994)075<1825:APFTIOI>2.0.CO;2)
- Kushner, P. J., & Polvani, L. M. (2006). Stratosphere–troposphere coupling in a relatively simple AGCM: Impact of the seasonal cycle. *Journal of Climate*, 19(21), 5721–5727. <https://doi.org/10.1175/JCLI4007.1>
- Labitzke, K., Massey, H. S. W., Beynon, W. J. G., Houghton, J. T., & Thomas, L. (1980). Climatology of the stratosphere and mesosphere. *Philosophical Transactions of the Royal Society of London - Series A: Mathematical and Physical Sciences*, 296(1418), 7–18. <https://doi.org/10.1098/rsta.1980.0152>
- Leibensperger, E. M., & Plumb, R. A. (2014). Effective diffusivity in baroclinic flow. *Journal of the Atmospheric Sciences*, 71(3), 972–984. <https://doi.org/10.1175/JAS-D-13-0217.1>
- Lin, S.-J. (2004). A “Vertically Lagrangian” finite-volume dynamical core for global models. *Monthly Weather Review*, 132(10), 2293–2307. [https://doi.org/10.1175/1520-0493\(2004\)132h2293:AVLFDCI2.0.CO;2](https://doi.org/10.1175/1520-0493(2004)132h2293:AVLFDCI2.0.CO;2)
- Linz, M. (2017). *Ngeo2017\_plots.m*. <https://doi.org/10.6084/m9.figshare.5229844.v1>
- Linz, M. (2021). Replication data for: Linz et al. 2021 stratospheric adiabatic mixing rates derived from the vertical gradient of age of air. *Harvard dataverse*. <https://doi.org/10.7910/DVN/GBRCWW>
- Linz, M., Abalos, M., Glanville, A. S., Kinnison, D. E., Ming, A., & Neu, J. L. (2019). The global diabatic circulation of the stratosphere as a metric for the Brewer–Dobson circulation. *Atmospheric Chemistry and Physics*, 19(7), 5069–5090. <https://doi.org/10.5194/acp-19-5069-2019>
- Linz, M., Plumb, R. A., Gerber, E. P., Haanel, F. J., Stiller, G., Kinnison, D. E., & Neu, J. L. (2017). The strength of the meridional overturning circulation of the stratosphere. *Nature Geoscience*, 10(663).
- Linz, M., Plumb, R. A., Gerber, E. P., & Sheshadri, A. (2016). The relationship between age of air and the diabatic circulation of the stratosphere. *Journal of Atmospheric Science*, 73(11), 4507–4518. <https://doi.org/10.1175/JAS-D-16-0125.1>
- Livesey, N. J., Read, W. G., Froidevaux, L., Lambert, A., Manney, G. L., Pumphrey, H. C., et al. (2011). *Earth observing system (eos) aura microwave limb sounder (mls) version 3.3 level 2 data quality and description document* (Tech. Rep. No. 3.3x-1.0). Pasadena, California: Jet Propulsion Laboratory.
- Mahieu, E., Chipperfield, M. P., Nothold, J., Reddmann, T., Anderson, J., Bernath, P. F., et al. (2014). Recent northern hemisphere stratospheric HCl increase due to atmospheric circulation changes. *Nature*, 515(7525), 104–107. <https://doi.org/10.1038/nature13857>
- Marsh, D. R., Mills, M. J., Kinnison, D. E., Lamarque, J.-F., Calvo, N., & Polvani, L. M. (2013). Climate change from 1850 to 2005 simulated in CESM1(WACCM). *Journal of Climate*, 26(19), 7372–7391. <https://doi.org/10.1175/JCLI-D-12-00558.1>
- McIntyre, M. E., & Palmer, T. N. (1984). The ‘surf zone’ in the stratosphere. *Journal of Atmospheric and Terrestrial Physics*, 46, 825–849. [https://doi.org/10.1016/0021-9169\(84\)90063-1](https://doi.org/10.1016/0021-9169(84)90063-1)
- McLandress, C., & Shepherd, T. G. (2009). Simulated anthropogenic changes in the Brewer–Dobson circulation, including its extension to high latitudes. *Journal of Climate*, 22(6), 1516–1540. <https://doi.org/10.1175/2008JCLI2679.1>
- Moore, F. L., Ray, E. A., Rosenlof, K. H., Elkins, J. W., Tans, P., Karion, A., & Sweeney, C. (2014). A cost-effective trace gas measurement program for long-term monitoring of the stratospheric circulation. *Bulletin of the American Meteorological Society*, 95(1), 147–155. <https://doi.org/10.1175/BAMS-D-12-00153.1>
- Morgenstern, O., Hegglin, M. I., Rozanov, E., O’Connor, F. M., Abraham, N. L., Akiyoshi, H., et al. (2017). Review of the global models used within phase 1 of the chemistry–climate model initiative (CCMI). *Geoscientific Model Development*, 10(2), 639–671. <https://doi.org/10.5194/gmd-10-639-2017>
- Neale, R. B., Richter, J., Park, S., Lauritzen, P. H., Vavrus, S. J., Rasch, P. J., & Zhang, M. (2013). The mean climate of the community atmosphere model (CAM4) in forced SST and fully coupled experiments. *Journal of Climate*, 26(14), 5150–5168. <https://doi.org/10.1175/JCLI-D-12-00236.1>
- Neu, J. L., & Plumb, R. A. (1999). Age of air in a “leaky pipe” model of stratospheric transport. *Journal of Geophysical Research*, 104(D16), 19243–19255. <https://doi.org/10.1029/1999JD900251>
- Newman, P. A., Schoeberl, M. R., & Plumb, R. A. (1986). Horizontal mixing coefficients for two-dimensional chemical models calculated from national meteorological center data. *Journal of Geophysical Research*, 91(D7), 7919–7924. <https://doi.org/10.1029/JD091iD07p07919>
- Ploeger, F., Abalos, M., Birner, T., Konopka, P., Legras, B., Müller, R., & Riese, M. (2015). Quantifying the effects of mixing and residual circulation on trends of stratospheric mean age of air. *Geophysical Research Letters*, 42, 2047–2054. <https://doi.org/10.1002/2014GL062927.1>
- Ploeger, F., Riese, M., Haanel, F., Konopka, P., Müller, R., & Stiller, G. (2015). Variability of stratospheric mean age of air and of the local effects of residual circulation and eddy mixing. *Journal of Geophysical Research*, 120(2), 716–733. <https://doi.org/10.1002/2014JD022468>
- Plumb, R. A. (2002). Stratospheric transport. *Journal of the Meteorological Society of Japan*, 80(4), 793–809. <https://doi.org/10.2151/jmsj.80.793>

- Plumb, R. A. (2007). Tracer interrelationships in the stratosphere. *Reviews of Geophysics*, *45*, 1–33. <https://doi.org/10.1029/2005RG000179>
- Plumb, R. A., & Ko, M. K. W. (1992). Interrelationships between mixing ratios of long-lived stratospheric constituents. *Journal of Geophysical Research*, *97*(D9), 10145–10156. <https://doi.org/10.1029/92JD00450>
- Polvani, L. M., & Kushner, P. J. (2002). Tropospheric response to stratospheric perturbations in a relatively simple general circulation model. *Geophysical Research Letters*, *29*(7), 40–43. <https://doi.org/10.1029/2001GL014284>
- Polvani, L. M., Wang, L., Abalos, M., Butchart, N., Chipperfield, M. P., Dameris, M., & Stone, K. A. (2019). Large impacts, past and future, of ozone-depleting substances on brewer-dobson circulation trends: A multimodel assessment. *Journal of Geophysical Research: Atmospheres*, *124*(13), 6669–6680. <https://doi.org/10.1029/2018JD029516>
- Putman, W. M., & Lin, S.-J. (2007). Finite-volume transport on various cubed-sphere grids. *Journal of Computational Physics*, *227*, 55–78. <https://doi.org/10.1016/j.jcp.2007.07.022>
- Randel, W. J., Wu, F., Vömel, H., Nedoluha, G. E., & Forster, P. (2006). Decreases in stratospheric water vapor after 2001: Links to changes in the tropical tropopause and the brewer-dobson circulation. *Journal of Geophysical Research*, *111*(D12), D12312. <https://doi.org/10.1029/2005JD006744>
- Ray, E. A., Moore, F. L., Rosenlof, K. H., Davis, S. M., Boenisch, H., Morgenstern, O., et al. (2010). Evidence for changes in stratospheric transport and mixing over the past three decades based on multiple data sets and tropical leaky pipe analysis. *Journal of Geophysical Research*, *115*(D21), D21304. <https://doi.org/10.1029/2010JD014206>
- Ray, E. A., Moore, F. L., Rosenlof, K. H., Davis, S. M., Sweeney, C., Tans, P., & Aoki, S. (2014). Improving stratospheric transport trend analysis based on SF<sub>6</sub> and CO<sub>2</sub> measurements. *Journal of Geophysical Research — D: Atmospheres*, *119*, 14110–14128. <https://doi.org/10.1002/2014JD021802>
- Ray, E. A., Moore, F. L., Rosenlof, K. H., Plummer, D. A., Kolonjari, F., & Walker, K. A. (2016). An idealized stratospheric model useful for understanding differences between long-lived trace gas measurements and global chemistry-climate model output. *Journal of Geophysical Research — D: Atmospheres*, *121*(10), 5356–5367. <https://doi.org/10.1002/2015JD024447>
- Rosenlof, K. H. (1996). Summer hemisphere differences in temperature and transport in the lower stratosphere. *Journal of Geophysical Research*, *101*(D14), 19129–19136. <https://doi.org/10.1029/96JD01542>
- Schoeberl, M. R., Douglass, A. R., Polansky, B., Boone, C., Walker, K. A., & Bernath, P. (2005). Estimation of stratospheric age spectrum from chemical tracers. *Journal of Geophysical Research*, *110*(D21), D21303. <https://doi.org/10.1029/2005JD006125>
- Solomon, S., Ivy, D. J., Kinnison, D., Mills, M. J., Neely, R. R., & Schmidt, A. (2016). Emergence of healing in the Antarctic ozone layer. *Science*. <https://doi.org/10.1126/science.aae0061>
- Sparling, L. C., Kettleborough, J. A., Haynes, P. H., McIntyre, M. E., Rosenfield, J. E., Schoeberl, M. R., & Newman, P. A. (1997). Diabatic cross-isentropic dispersion in the lower stratosphere. *Journal of Geophysical Research*, *102*(D22), 25817–25829. <https://doi.org/10.1029/97JD01968>
- US Environmental Protection Agency (2016). *Climate change indicators in the United States* (4th ed.,). EPA 430-R-16-004 Retrieved from <https://www.epa.gov/climate-indicators>
- Vogel, B., Müller, R., Günther, G., Spang, R., Hanumanthu, S., Li, D., et al. (2019). Lagrangian simulations of the transport of young air masses to the top of the asian monsoon anticyclone and into the tropical pipe. *Atmospheric Chemistry and Physics*, *19*(9), 6007–6034. <https://doi.org/10.5194/acp-19-6007-2019>
- von Clarmann, T., & Grabowski, U. (2016). Direct inversion of circulation and mixing from tracer measurements – Part 1: Method. *Atmospheric Chemistry and Physics*, *16*(22), 14563–14584. <https://doi.org/10.5194/acp-16-14563-2016>
- Waugh, D., & Hall, T. M. (2002). Age of stratospheric air: Theory, observations, and models. *Reviews of Geophysics*, *40*(4), 1010. <https://doi.org/10.1029/2000RG000101>